Available online at www.sciencedirect.com
SCIENCE DIRECT®
Coordination Chemistry Reviews 248 (2004) 1165–1179
COORDINATION CHEMISTRY REVIEWS
www.elsevier.com/locate/ccr

Review

Electrons in nanostructured TiO_2 solar cells: transport, recombination and photovoltaic properties

Arthur J. Frank*, Nikos Kopidakis, Jao van de Lagemaat

National Renewable Energy Laboratory, 1617 Cole Blvd., Golden, CO 50801-3393, USA

Received 20 October 2003; accepted 9 March 2004
Available online 28 May 2004

Contents

Abstract

This review highlights several significant advancements in understanding of electron transport and recombination in dye-sensitized nanostructured TiO_2 solar cells and the limitations that these processes impose on cell performance. The influences of the electrolyte composition, network morphology, defect structure, and light intensity on the electron transport dynamics are evaluated. Also assessed are evidences for and implications of the large, spatially distributed nanoparticle–electrolyte interfaces, trap-state distribution, band-edge movement, and the redox electrolyte on the recombination kinetics. The theoretical PV characteristics of a dye-sensitized solar cell are compared with those of the highest confirmed efficiency cells and the fundamental factors that limit their performance are discussed.

Keywords: Grätzel cell; Dye sensitization; Transport; Recombination; Photovoltaic properties

1. Introduction

About 10 years ago, Grätzel and O'Regan published an article in Nature [1] that described a remarkably efficient photochemical solar cell based on the dye sensitization of mesoporous nanocrystalline titanium dioxide films. This new type of solar cell technology offered the promise of achieving moderate efficiency devices at ultra-low costs. The possibility of exploiting this technology has stimulated the interest of several major companies. In recognition of his pioneering work, this type of solar cell is often called a Grätzel cell. Besides stimulating industrial interest, the Grätzel cell raised important scientific questions about the fundamental processes governing its operation. As band bending and

* Corresponding author. Tel.: +1-303-384-6262; fax: +1-303-384-6150.
E-mail address: afrank@nrel.gov (A. J. Frank).

0010-8545/$ – see front matter © 2004 Elsevier B.V. All rights reserved.
doi:10.1016/j.ccr.2004.03.015

the formation of a depletion layer were considered unlikely in nanocrystalline TiO_2 electrodes owing to the extremely small size of the particle [2,3], much of the analysis developed previously to describe the photoelectrochemical behavior of planar semiconductor electrodes could not be applied in a straightforward fashion to nanostructured films. For instance, the photovoltage mechanism was indiscernible. The relation between the surface area of the TiO_2 nanoparticle film and the photovoltage was puzzling at the time. Although the large surface area of the nanoparticle film used in the cell could account for the observed photocurrent, it could not explain the magnitude of the observed photovoltage. It was also difficult to understand how electrons could move through insulating particles to the collecting electrode without undergoing significant recombination, which would have markedly deteriorated the photovoltaic response of the cell.

In this article, we review the current understanding of electron transport and recombination in nanostructured TiO_2 solar cells and discuss the limitation that they impose on cell performance. While much progress has been made in advancing the scientific knowledge of transport and recombination phenomena in porous nanostructured electrodes over the past several years, even today several important issues are still not well understood.

To reduce unavoidable overlap with other review articles in this volume, we restrict our discussion to studies of fully functional Grätzel cells that contain all of the components necessary for them to be regenerative. The typical Grätzel cell can be viewed as consisting of two percolating continuous random networks [4]: a network of TiO_2 nanoparticles and a "negative" network of pores filled with an organic liquid (or polymer) electrolyte. The dye molecules attached to the TiO_2 surface resides at the interface of the two networks. The TiO_2 nanoparticles, which are depleted of electrons in the dark, serve to transport electrons to a transparent conducting oxide (TCO; $F:SnO_2$) substrate—the collecting electrode. Because of the small particle size (~20 nm), the surface area (roughness factor) of the film is more than a thousand times that of a flat electrode of the same size. The TiO_2 network is the recipient of injected electrons from optically excited dye molecules and provides the conductive pathway from the site of electron injection to the collecting electrode. The electrolyte in the pores, which is normally of high ionic strength, serves to transport holes in the form of a redox carrier (e.g., I_3^-) from the oxidized dye to the counter electrode, where they are reduced by the collected electrons via the external circuit.

Section 2 of this paper provides a brief description of the experimental techniques employed in the investigation of transport and recombination. Sections 3 and 4 discuss the evidence and models that are invoked to explain the transport and recombination kinetics, and the photocurrent and photovoltage mechanisms. In Section 5, the theoretical PV characteristics of a dye-sensitized solar cell are compared with those of the highest confirmed efficiency Grätzel cells and the fundamental factors that limit their performance are discussed.

2. Experimental techniques

In the past decade, considerable insight into the kinetics and energetics of transport and recombination in dye-sensitized solar cells has been achieved by using frequency- and time-domain techniques, such as intensity modulated photocurrent spectroscopy (IMPS) [5–13], intensity modulated photovoltage spectroscopy (IMVS) [11,14,15], electrical impedance spectroscopy (EIS) [11,16–21], transient photocurrent [4,5,16,22–29], and transient photovoltage [29,30]. The frequency domain techniques measure the response (or recovery) of a system to a small periodic perturbation, whereas the transient technique measures the response of a system to small temporal perturbation. There are also several transient studies of the Grätzel cell involving large perturbations [22,31,32], although they are not discussed in this review. Both frequency- and time-domain studies yield the same information. However, each technique has its own advantages and disadvantages. For example, working in the time domain is more intuitive for many because it relates to our normal, everyday perception of causality. On the other hand, it can be convenient to apply a modulation technique to investigate the prediction of a model with expressions more easily solvable in frequency space than in the time domain. Mathematically, data gathered in the frequency and time domains are interconvertible.

Intensity-modulated photocurrent spectroscopy probes the modulation of the photocurrent in response to the modulation of light intensity. This technique is usually performed at short circuit, although it can also be applied under potentiostatic conditions [11]. The modulated light intensity is superimposed on a base (bias) light intensity, which produces a steady-state photocarrier density. The IMPS function $(\Delta\tilde{J}/(q\,\Delta\tilde{\phi}_0))$ is the complex ratio of the current response $\Delta\tilde{J}$ to incident light intensity modulation $\Delta\tilde{\phi}_0$. The IMPS technique has been used to estimate the electron diffusion coefficient D_n in dye-sensitized TiO_2 films at short circuit. In one study [7], the authors solved the frequency-dependent diffusion (continuity) equation and fitted the resulting IMPS response to the experimental data to determine values for the effective diffusion coefficient and electron lifetime.

At low modulation frequencies, the IMPS function can be expressed in terms of a single equation:

$$\frac{\Delta\tilde{J}}{q\,\Delta\tilde{\phi}_0} = A\frac{1}{1+\mathrm{i}\omega\tau_c} \tag{2.1}$$

where τ_c is the time constant for electron collection at short circuit in the absence of recombination and when electron transfer across the TiO_2–TCO interface is much faster than electron transport. Eq. (2.1) represents a single semicircle in the complex plane corresponding to a single time constant for electron collection [23]. At short circuit, τ_c can be viewed

as the average time for electron collection. The time constant for electron collection is related to the electron diffusion coefficient by the expression [23]:

$$\tau_c \approx \frac{d^2}{2.35 D_n} \tag{2.2}$$

In the absence of recombination, the steady-state electron charge Q_{tot} in the film at short circuit has been estimated as the product of τ_c and the short-circuit photocurrent density J_{sc}:

$$Q_{tot} = J_{sc}\tau_c \tag{2.3}$$

Intensity modulated photovoltage spectroscopy measures the modulation of photovoltage at open circuit $\Delta\tilde{V}_{oc}$ in response to the modulation of the incident light intensity. For pseudo first-order kinetics, the decay of the open-circuit photovoltage is determined by a single time constant $1/\omega_{min}$, which corresponds to the lifetime τ_r for recombination of electrons with oxidized species in the electrolyte [9,15]. The steady-state electron charge in the film at open circuit has been estimated as the product of τ_r and J_{sc} [9,15].

In the transient photocurrent technique, the steady-state photocarrier density, which is established by a bias light, is perturbed by a weak probe pulse. Measurement of the response of the photocurrent to the probe pulse yields information on the characteristic time for electron diffusion (collection) [4,22,23,29]. In complete analogy with the IMPS response (Eq. (2.1)), the photocurrent response can be represented at long time by a single equation ($J(t) = A'e^{-t/\tau_c}$, where A' is a constant) and a single time constant τ_c [4,23,29]. In transient photovoltage measurements an exponential decay of the photovoltage is observed with a single time constant τ_r.

Electrical impedance spectroscopy is another technique for studying transport and recombination in dye-sensitized TiO_2 nanocrystalline films [11,17–21]. EIS measures the current response to a modulated applied bias superimposed on a constant applied voltage. The impedance is defined as the ratio of the voltage modulation to the current response and is typically modeled by an equivalent electrical circuit [11,17–20]. An equivalent circuit of the sensitized TiO_2 photoelectrode, which takes into account the conducting glass–TiO_2 interface and the TiO_2–redox electrolyte interface, provides a very good description of the observed impedance spectra [11]. Interpretation of the impedance spectra using such an equivalent circuit can provide direct information about the recombination time of electrons with the redox electrolyte at any bias, the electrical and electrochemical potential distribution, and the energy distribution of surface or other trap states in illuminated cells [11].

Intensity modulated infrared transmittance spectroscopy (IMIS) is an experimental technique which does not probe photocarrier transport directly but is used to supplement transport and recombination measurements [33,34]. IMIS measures the infrared transmittance response of a cell to modulation of the incident visible light intensity. The IMIS technique combined with IMPS and IMVS measurements at short circuit or open circuit, respectively, provide information about the spatial distribution of photocarriers in a device.

3. Electron transport dynamics

Transport along with recombination is a major determinant of the overall performance of the Grätzel cell. This section describes the evidence for several important factors, including the electrolyte composition, the network morphology, and the defect structure and the light intensity, that governs electron transport in electrolyte-filled mesoporous nanoparticle networks. We first consider the consequence of the electrolyte composition on the kinetics and energetics of transport.

3.1. Ambipolar diffusion

The transport of injected electrons through the TiO_2 nanoparticle layer to the collecting electrode is believed to occur by diffusion because the *macroscopic* electric field across the film is negligible at solar light intensities up to one sun due to screening by the high ionic strength electrolyte [23]. In Section 3.2, we examine the effect of light intensities at or above one sun at which the macroscopic electric field is not negligible across the film [35,36]. The use of high ionic strength electrolytes ensures that electroneutrality is obeyed throughout the network [11,22,24,37] and that ion diffusion is strongly correlated with electron transport [22,24,38]. The length scale over which electroneutrality in the electrolyte is maintained is given by the Debye length, which is of the order of 0.1 nm. As ions do not readily infuse into a particle lattice, save for intercalation, the Debye length that electrons experience is comparable to the radius of a single particle or less as the number of electrons increases above one per particle. The principal consequence of electroneutrality is that the diffusion of electrons is ambipolar [22,38]; such transport is also known as chemical or mutual diffusion [39]. The motion of electrons creates a charge imbalance, and the resulting electric field drags the cations along with them. At the same time, negatively charged ions are repelled from the electrons. The net effect is that diffusion of electrons is retarded, and the diffusion of ions is increased. The reverse effect must also be considered in which the diffusion of electrons is increased and the diffusion of ions is slowed. Thus, the simultaneous motion of electrons and ions yields a single diffusion coefficient owing to their inseparable motion [22]. Ambipolar diffusion also occurs in compact semiconductors [40] and in plasmas. A simplified expression for the ambipolar diffusion coefficient of charge transport has been proposed to describe transport in electrolyte-filled mesoporous TiO_2 films [22,41]:

$$D_{amb} = \frac{n + p}{n/D_p + p/D_n} \tag{3.1}$$

where D_p represents the diffusion coefficient of ions and p and n are the respective densities of ions and electrons. Recently, Eq. (3.1) was shown to account for the electron diffusion coefficient dependence on the ionic strength of the electrolyte [42,43]. In reality, the electrolyte is composed of both negatively and positively charged species of various types. A recent paper explores this effect on transport in detail [38].

There are several consequences of ambipolar diffusion for the Grätzel cell. First, electron and ion transport are inseparable on a length scale larger than that of a single particle. However, because the electron concentration ($n < 10^{18}\,\mathrm{cm}^{-3}$) in TiO_2 films is generally much less than the ion concentration (p of the order of $10^{21}\,\mathrm{cm}^{-3}$) in a high ionic strength electrolyte, the ambipolar diffusion coefficient is, to a very good approximation, the same as the diffusion coefficient of electrons ($D_{amb} = D_n$, Eq. (3.1)) [22]. Thus, for all practical purposes, the measured diffusion coefficient and the electron diffusion coefficient are the same. Second, electrons can be detected only after they reach the collector. This means that the current measured in the external circuit correlates with the arrival of electrons at the collecting electrode, in contrast to many solid-state devices where the current is the result of electron motion in the semiconductor (a displacement current). Although several groups [7,9,24] have intuitively interpreted their charge transport measurements as reflecting arrival time detection, it is actually a consequence of ambipolar diffusion. The situation for the Grätzel cell is closely analogous to the historic Haynes–Shockley experiment, where the ambipolar drift of electrons in p-type Ge was shown to occur [22,41,44].

It is informative to examine the validity of the argument that ambipolar diffusion is incongruous with multiple trapping kinetics (Section 3.3). In particular, it can be argued that an electron resides in a deep trap much longer than the reorganization time of ions in the electrolyte. Upon emission to the conduction band, the electron supposedly diffuses so rapidly that its velocity is limited only by the Debye relaxation of both the polar TiO_2 lattice and the electrolyte, which shields the electron from any electrical field caused by a charge imbalance in the electrolyte. The fallacy of this argument is that the ions in the electrolyte establish a (quasi) static potential energy well inside the TiO_2 that still retards the electron from advancing from its original position however fast it moves. A high frequency ac field, such as that produced by the dielectric relaxation, cannot shield the field caused by slow relaxation of the electrolyte because it cannot generate a charge density over length scales larger than a few atoms.

3.2. Film morphology

Several studies have examined the influence of film morphology on electron transport. It has been found that electron transport in rutile TiO_2 layers is about an order of magnitude slower than transport in anatase TiO_2 [45]. This difference in transport rate is attributed to a smaller number of interconnects between particles owing to the more open rod-like morphology of the rutile layers. As another example of the importance of film structure in transport, the influence of the overlap between neighboring particles on electron transport has been investigated. Electron transport through a string of spheres was modeled as a function of the interconnecting areas between the spheres [46]. It was found that the smaller the area of interconnect, the slower is the overall transport. Besides the interconnect between two particles, a film has a larger scale structure defined by how the particles are arranged in a network. In a real nanoparticle film, each particle is coordinated, on average, with more than two particles, and the film is more accurately depicted as a random network with a random number of interconnections at each particle, which may be likened to a "hub" [4,47]. A recent study has modeled TiO_2 films as random particle network [4]. It was shown that the coordination number of individual particles in a network varies strongly with the film porosity and is a broadly distributed quantity at a given porosity. The *average* coordination number of a particle ranges from about 2.5 at 75% porosity to about 5 at 50% porosity [4,47].

The electron transport dynamics have been modeled using simulated mesoporous *random* nanoparticle TiO_2 films and the random-walk approach [4]. Diffusion (random walk) in such networks was described in terms of percolation theory, which predicts a power-law dependence (exponent μ) of the diffusion coefficient on the difference between the film *porosity* (P) and some critical *porosity* (P_c):

$$D \propto |P_c - P|^{\mu} \tag{3.2}$$

Fig. 1 shows that the random-walk simulations of electron transport and experimental data are in quantitative agreement with each other. From the analysis of the data, the critical porosity P_c (percolation threshold) and the conductivity exponent μ were found to be 0.76 ± 0.01 and 0.82 ± 0.05, respectively. The fractal dimension of the nanoparticle films was estimated from the simulations to be 2.28, which concurred with gas-sorption measurements [4]. These results imply that the simulated films serve as a good model for actual nanoparticle films. It was estimated that during their respective transit through 50 and 75% porous 10 μm thick films of 20 nm particles, the average number of particles visited by electrons increases by 10-fold, from 10^6 to 10^7, indicating that with higher porosity films the electron transport pathway becomes longer, even though there are less particles present per volume area. In contrast, when the particles are arranged in a simple cubic lattice, which has porosity of 48%, the average electron visit only 6×10^5 particles [4]. Therefore, the effect of the randomness of the film is to almost double the length of the electrons pathway. For higher porosity films, corresponding to lower average coordination numbers, there are more isolated areas in the film that are only connected to the rest of the film by a single particle that acts as a nexus. These isolated areas act as spatial electron traps that slow electron transport [4].

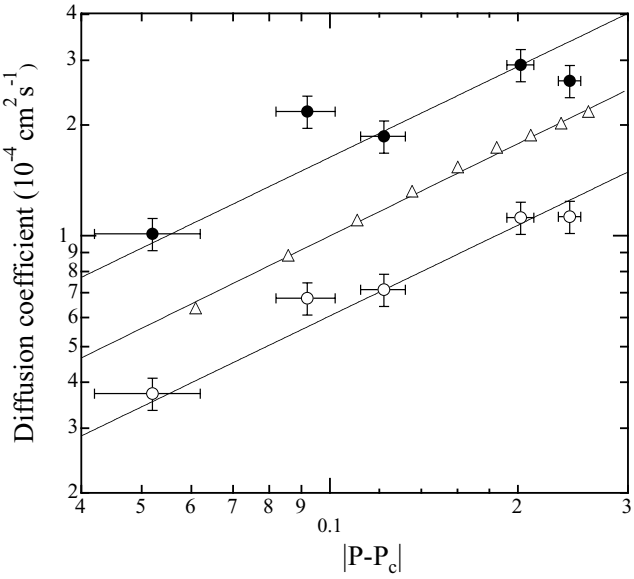

Fig. 1. Dependence of diffusion coefficient on film porosity. Triangles depict random-walk simulations on a computer-simulated nanoparticle network, and the circles show experimental results with two electrolytes (tetrabutylammonium iodide and 1-hexyl-2,3-dimethylimidazolium iodide). Continuous lines show fits to Eq. (3.2) using the same values for P_c and μ for each plot. Adapted from [4].

3.3. Multiple trapping

It was first observed in 1991 [25] that electron transport in dye-sensitized cells depends strongly on light intensity. This dependence was attributed to a broad distribution of traps. Other researchers have confirmed the light-intensity dependence and have explained it in terms of a multiple trapping model [5–13]. Fig. 2 shows a typical dependence of the ambipolar diffusion coefficient on photocarrier density,

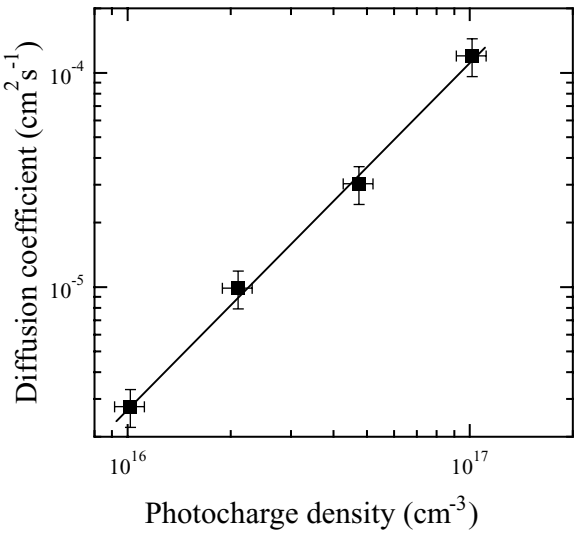

Fig. 2. Dependence of measured ambipolar diffusion coefficient on photoinjected charge density in the TiO_2 film. Continuous line is a fit to a power-law relation (Eq. (3.4)).

which was estimated from the product of the short circuit photocurrent density and the collection time constant of electrons) [12,22,23]. The absolute magnitude of the electron (or more correctly, the ambipolar) diffusion coefficient for dye-sensitized nanoparticle TiO_2 films is observed to be several orders of magnitude lower than it is for single crystal anatase [22,24,48]. While interparticle necking [46] and the network topology of the TiO_2 films [4] can account for the lower value of the diffusion coefficient, neither can explain the light-intensity dependence of the diffusion coefficient. The dependence of the diffusion coefficient on the photocarrier density is found to follow a power law with an exponent ranging between 1 and 17 [29]. This power-law behavior has been explained in terms of electrons performing an exclusive random walk between localized sites that have a power law distribution of waiting times $\psi(t)$ [23,49–52]:

$$\psi(t) \propto t^{-1-\alpha} \tag{3.3}$$

where α is a dispersion parameter with a value between 0 and 1. When a certain density of electrons performs a simultaneous random walk over such a distribution of waiting times, the few "states" with the longest waiting times are filled, causing the distribution of times to be modified by a "knee" beyond which there are fewer available "states" [23]. This leads to a strong dependence of the diffusion coefficient on the photoinjected electron density n having the form [22,23]:

$$D_n \propto n^{(1-\alpha/\alpha)} \tag{3.4}$$

From analyses of D_n versus n plots, it is estimated that the dispersion parameter α ranges from 0.06 to 0.5 [29]. A waiting-time distribution depicted by Eq. (3.3) can represent the disorder in activation energies for intersite transport, carrier locations or both [49,51]. In the case of energetic disorder, carriers are emitted thermally from a distribution of trap states, whereas for positional disorder, carriers tunnel (or hop) between localized sites. In the latter case, their waiting time is determined by the distance between nearest neighboring sites and the energy difference between sites, both of which are characterized by a broad distribution. This type of transport is often referred to as variable range hopping [53]. Currently, only the energetic disorder model has been applied to explain electron transport in TiO_2 nanoparticle films, although there is no definitive experimental evidence that distinguishes between the two models.

Fig. 2 illustrates the power-law dependence of D_n on n determined from transient photocurrent measurements. To account for such behavior with the energetic disorder model, the energy distribution of trap states g(E) would have an exponential form [12,22,23,51]:

$$g(E) = g_0 \exp\left(\alpha \frac{E - E_c}{kT}\right) \tag{3.5}$$

where E is the trap energy, E_c the conduction band edge energy, and the parameter g_0 a constant. The parameter α, which describes the steepness of the trap-state distribution, is related to the average trap depth m_c by the equal-

ity: $\alpha = kT/m_c$. Multiple trapping of carriers involving an exponential trap distribution has also been invoked to account for transport in amorphous and polycrystalline materials [54,55]. At steady state, the equilibration of empty and trap-filled states establishes a quasi-Fermi level. The occupancy of a trap level is described by Fermi–Dirac statistics:

$$f(E) = \left[1 + \exp\left(\frac{E - \bar{\mu}_n}{kT}\right)\right]^{-1} \quad (3.6)$$

where $f(E)$ is the Fermi–Dirac function and $\bar{\mu}_n$ the electrochemical potential of electrons, which is equal to their quasi-Fermi level. It is straightforward to show that for thermally activated emission from traps, the waiting-time distribution (Eq. (3.3)) and, therefore, the power-law dependence of electron diffusion on the photocarrier density (Eq. (3.4)) can be obtained by combining the expressions for an exponential distribution of trap energies (Eq. (3.5)) and Fermi–Dirac statistics (Eq. (3.6)) with the assumption that the detrapping time is much longer than the intertrap diffusion time [12,22,23]. The rationale for this is that at higher photocharge density, the traps are filled to a higher level (the quasi-Fermi level) and only traps at or above this level participate in electron transport. With fewer available deep traps, transport becomes faster. An exponential density of states has also been assumed for other nanostructured semiconductors, such as rutile TiO_2 [45], zinc oxide [56], and gallium phosphide [57] interpenetrated with an electrolyte.

At present, the origin of an exponential density of states in TiO_2 remains an elusive issue, especially because the spectroscopic evidence for electron traps in TiO_2 points to localized energy states [58–62]. There is also a study that indicates that most of the electrons in anatase TiO_2 are free [61], implying that traps do not retard transport. However, most of the transport measurements point to an exponential distribution of trap states. It is, therefore, informative to speculate about possible causes for an exponential conduction band tail. In analogy with disordered materials, such as amorphous or polycrystalline silicon, the band tail could be due to structural disorder, grain boundaries, interfaces, charged defects, etc. [63,64]. Recently, it has been shown that intercalating small amounts of Li^+ ions (about 50 per particle) into TiO_2 films markedly slows electron transport [29]. Concomitantly, the slope of the D versus n curves dramatically increases, indicating that α becomes smaller, corresponding to a steeper trap-state distribution [22,29]. This behavior is consistent with widening of the exponential conduction band tail resulting from disorder induced by randomly placed lithium (ionized) defects in TiO_2, which, in turn, creates random Coulomb potential fluctuations [64]. In other words, because of random placement of Li^+, some defects could exist as single ions while others could occur in close association, which would create deeper traps. Presumably, in the absence of intercalated Li^+, intrinsic defects or defects at grain boundaries or surfaces would lead to the exponential density of states. Another possible explanation for an exponential density of state arises from the fact that entirely different materials, such as TiO_2 (both anatase and rutile), ZnO, and GaP, all exhibit similar power-law behavior [45,56,57]. Each of these large bandgap semiconductors is a polar material, which results in strong electron–phonon interaction and consequently exponential absorption tails owing to self-trapped exciton formation [65]. In the case of anatase, these absorption tails have similar slopes to those proposed to explain the transport results [65]. It is difficult, however, to understand how such a mechanism could lead to the filling effects (i.e. light-intensity dependence) observed in the electron transport dynamics. Also, electron–phonon coupling is already incorporated in the mobility of quasi-free electrons [48].

Recently, a mechanism that does not involve an exponential trap-state distribution has been proposed to explain the observed kinetics in TiO_2 nanoparticle films [66]. Based on evidence for surface trap states in rutile TiO_2 [62], which probably has a similar defect structure to anatase, the authors suggest that a combination of two Gaussians centered at trap energies of about 0.32 and 0.5 eV below the conduction band can also explain the observed power-law relation. These states are attributed to oxygen vacancies and their first ionization state [62]. In Fig. 3a, we plot the best-fit values for the two Gaussians [66] together with an exponential density of states (Eq. (3.5)) for $\alpha = 0.31$. A comparison reveals that over a range of energies, corresponding to the Fermi level positions found for the Grätzel cell, the two functions have similar slopes. Fig. 3b also shows that the two Gaussians and exponential density of states result in similar waiting-time distributions, indicating that the exponential and Gaussian distributions are approximately equivalent with respect to the light-intensity dependence of steady-state electron diffusion and that it is experimentally difficult to distinguish between them.

3.4. Thermodynamic driving force

Electron transport is believed to be purely diffusional. It is, however, possible that the charging of TiO_2 nanoparticles results in a band-edge shift [15,35], which causes the buildup of an electrical field across the TiO_2 layer because of the electron concentration dependence on position [35]. This electrical field has been shown to serve as an additional driving force for electron transport [35] and can increase the apparent diffusion coefficient by approximately 10% at one-sun light intensity [36]. The magnitude of this driving force has been derived for a non-exponential trap distribution [35]. As most of the studies reviewed assume an exponential trap-state distribution, we give the equivalent result here for consistency. It is shown that at operating conditions of the Grätzel cell, the contribution of this additional driving force is significant. Although not considered in this paper, a similar approach can lead to expressions describing ambipolar (or mutual or chemical) diffusion [67].

A comprehensive description of electron transport must take into account transport driven by both concentration gra-

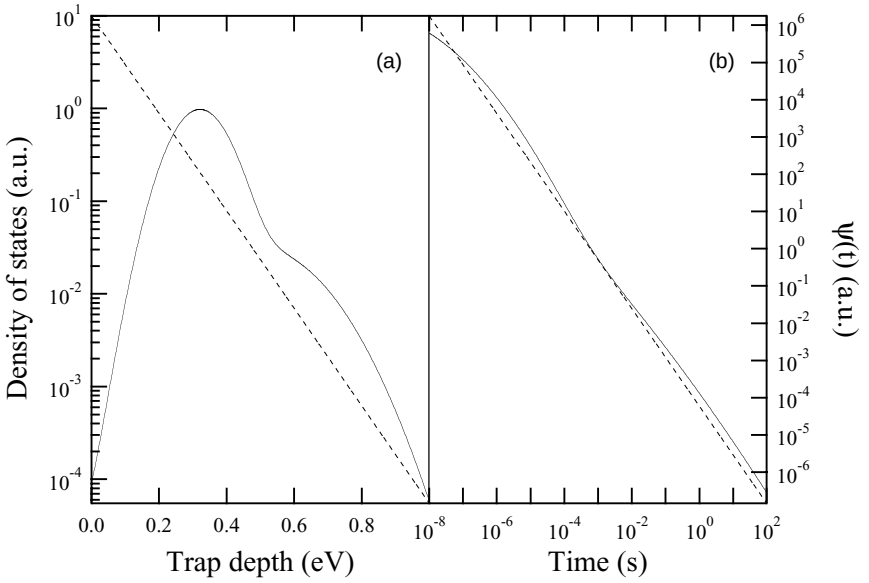

Fig. 3. (a) Comparison of exponential distribution of states (Eq. (3.5)) for $\alpha = 0.31$ (dashed line) and a distribution of states formed by summing two Gaussian peaks as described in [66] (continuous line). The best-fit values from [66] were used to calculate the Gaussian distributions. (b) Waiting-time distributions correspond to the two distributions displayed in (a).

dients and electrical fields. It is convenient to express the gradient of the electrochemical potential as a thermodynamic driving force [35,67,68]. The electron flux J_n is given by expression:

$$J_n = -nm_n \frac{\nabla \bar{\mu}_n}{q} \tag{3.7}$$

where m_n is the electron mobility, $\bar{\mu}_n$ the electrochemical potential, and ∇ is the spatial gradient operator given by $\nabla = \partial/\partial x + \partial/\partial y + \partial/\partial z$. The term $\nabla\bar{\mu}_n/q$ is the driving force F_n for electron transport ($F_n = (\nabla\mu_n/q) - E$), which is the sum of a field driven term ($E = \nabla\varphi$) and a chemical potential gradient term ($\nabla\mu_n$) inasmuch as the electrochemical potential is the sum of an electrical (φ) and a chemical potential contribution [35]. At constant pressure and temperature, the driving force for electron transport is given by the product of the concentration dependence of the electrochemical potential and the concentration gradient of electrons [35,67,69]:

$$F_n = \frac{kT}{q} \underbrace{\left(\frac{\partial \bar{\mu}_n/kT}{\partial \ln n}\right)_{P,T}}_{\text{thermodynamic factor } T_n} \frac{\nabla n}{n} \tag{3.8}$$

With the aid of Eq. (3.8), the electron flux (Eq. (3.7)) can be expressed as [70]:

$$J_n = -D_{\mathrm{RW}} T_n \nabla n = -D_{\mathrm{ch},n} \nabla n \tag{3.9}$$

where the Einstein relation between mobility and random-walk diffusion coefficient $D_{\mathrm{RW}} = (kT/q)m_n$ is used. Eq. (3.9) is Fick's first law of diffusion for which the effective (chemical) diffusion coefficient $D_{\mathrm{ch},n}$ is obtained by combining the thermodynamic factor T_n and the diffusion coefficient D_{RW}. Eq. (3.9) shows that any extra driving force, such as a band-edge shift, leads to a change of the effective diffusion coefficient $D_{\mathrm{ch},n}$ so that the overall electron transport still appears to be diffusion-controlled [36]. The effective diffusion coefficient differs from the *random-walk* diffusion coefficient (the Einstein relation) by a thermodynamic factor that describes particle–particle interactions [69].

In the absence of significant band bending, charging of the Helmholtz layer lowers the electrical potential inside the TiO_2 particles at a certain position in the film by a factor of qn/c_{H} [35], where c_{H} is the capacitance density, which equals the product of the density of the surface area of the film (surface area/unit volume; typically, ca. $10^6\,\mathrm{cm}^{-1}$) and the Helmholtz capacitance at the TiO_2 surface (typically, ca. $10^{-5}\,\mathrm{F\,cm}^{-2}$). The c_{H} value of a TiO_2 film is normally about $10\,\mathrm{F\,cm}^{-3}$. From Eqs. 3.5, 3.6, and 3.8, it follows that the thermodynamic factor T_{n} for an exponential trap-state distribution is:

$$T_n = \frac{(\partial \bar{\mu}_n/kT)}{\partial \ln n} = \frac{1}{\alpha} + \frac{q^2 n}{kTc_{\mathrm{H}}} \tag{3.10}$$

The small difference between Eq. (3.10) and the relation in the literature [35] is due to the assumption of an exponential density of states in the current treatment. The $1/\alpha$ term, which relates to the steepness of the trap-state distribution and is independent of light intensity, typically ranges from 3 to 4 but can be as high as 17 under special conditions [29]. In the case of a flat density of states, the first term in Eq. (3.10) equals unity [35]. The second term, which depends strongly on the photoinjected electron density, is the

cause of the increased driving force at high light intensities [35,36]. For instance, at a photoinjected electron density of 10^{17} and $10^{18}\,cm^{-3}$, which corresponds to about one-sun light intensity, the electrical component of the driving force (the second term in Eq. (3.10)) is between 2 and 20% of the diffusional component (the first term in Eq. (3.10)) for the normal range of $1/\alpha$. Thus, at one-sun light intensity, the electrical field created by band-edge movement in conventional Grätzel cells can produce a significant increase (2–20%) of the apparent diffusion coefficient (Eq. (3.9)). In future high efficiency Grätzel cells and cells operating above one-sun light intensity this effect is expected to be even more important. Unfortunately, the influence of an additional (electrical) driving force on the effective diffusion coefficient is not readily amenable to experimental investigation because transport still appears to be diffusion controlled, i.e., Fick's first law of diffusion is still obeyed.

4. Recombination kinetics

Recombination of photocarriers (or, equivalently, back electron transfer) in a conventional Grätzel cell refers to the process in which photoinjected electrons are transferred across the TiO_2 nanoparticle–electrolyte interface to oxidized species of the redox couple. Although electron transfer to the oxidized dye occurs under some circumstances [71,72], it is negligible in a normal Grätzel cell containing the standard I_3^-/I^- redox couple [29,73]. The characteristic time for recombination in this cell under normal illumination conditions can range from milliseconds to minutes, depending on the light intensity [9,15,29,31]. It is notable that electrons in TiO_2 nanoparticle films, separated from oxidizing species in the electrolyte by only nanometers, can survive for such long time periods without recombining [22,73]. As transport is generally an order of magnitude faster than recombination, the charge-collection efficiency in conventional cells is typically close to unity at one-sun light intensity [9,11]. A major reason for the good performance of the conventional Grätzel cell is the relatively slow recombination kinetics of the I_3^-/I^- redox couple [73]. The net recombination reaction can be expressed as follows:

$$I_3^- + 2e^- \rightarrow 3I^- \tag{4.1}$$

Several important issues have been investigated relating to the recombination reaction. These include questions about its location within the cell, the trap-state distribution, band-edge movement, and its mechanism. The answers to these questions provide not only scientific insight into the nature of the recombination reaction but also guidelines for controlling it. In the following, we review investigations of these issues and the evidence for models that have been proposed to understand it. By examining these models as well as some recent results, an understanding of the principal features of the recombination mechanism emerges.

4.1. Locus of recombination

In principle, recombination can take place at several interfaces: the TiO_2 nanoparticle–electrolyte interface, TiO_2–TCO interface, and TCO electrolyte interface or some combination of them. The interface, where recombination predominates, is dependent on the redox electrolyte and the surface properties of both the TCO (SnO_2) substrate and TiO_2. We first consider dye-sensitized TiO_2 solar cells with the standard I_3^-/I^- couple. The locus of recombination is related to where charge builds up in the cell, which, in turn, influences the photovoltage mechanism and the cell performance. Analyses of IMVS results [15] indicate that photoinjected electrons buildup in the nanoparticle TiO_2 film and that the photopotential of the cell originates from the change of the quasi-Fermi level of the TiO_2 film in response to the buildup of charge. Electrical impedance spectroscopy measurements of the cell in the dark at forward bias, when electrons flow into the film from the TCO contact, show [37,74] that a bias dependent capacitance develops at the TiO_2 nanoparticle–electrolyte interface, which is also consistent with charging of the film. EIS studies [11] of the cell under one-sun illumination show that the capacitance increases exponentially with applied forward bias, reaching values of several mF/cm^2 at open circuit. Such a large amount of charge would be difficult to associate with the narrow spatial region of the TiO_2–TCO interface and has consequently been attributed to charging of surface states of the nanoparticle film. From the EIS studies, it has also been concluded that the photovoltage of the Grätzel cell is caused by the rise in the Fermi level in the TiO_2 film owing to the buildup of charge. The results of the EIS study are in discordance with a diffusion diode model [20,21], which would predict that the capacitance C varies with the applied bias V_b according to the relation $C \propto \exp(V_b/kT)$, which is contrary to observations ($C \propto \exp(V_b/110\ mV)$) [11]. Furthermore, the impedance studies [11] show that the kinetic limiting process in these cells occurs at the TiO_2–electrolyte interface (as a result of recombination) instead of at the TCO–TiO_2 interface. Other impedance studies have reached the same conclusion about the location for recombination [19].

The reduction of the oxidized component of the I_3^-/I^- couple occurs relatively slowly on both the SnO_2 and TiO_2 surface. However, a recent study has shown that with simple one-electron redox couples, such as ferrocenium/ferrocene, the oxidized redox species is reduced much faster on the SnO_2 surface than on the TiO_2 surface in the dark, indicating that the overpotential for ferrocenium reduction at the TCO surface is much less than that for large surface area porous TiO_2 nanoparticle films [73]. In contrast, the overpotential for reducing the oxidized component of the

I^-/I_3^- couple is less at the surface of porous TiO_2 nanoparticle films than at the TCO surface, which is consistent with recombination occurring predominantly at the TiO_2–redox electrolyte interface [73]. A substantial loss of both the photocurrent and photovoltage has been observed when recombination occurs primarily at the TCO surface. Passivating the surface of the SnO_2 substrate with an insulating polymer film has been shown to improve the PV properties of cells with a fast redox couple. In contrast, passivating the TCO surface has no effect on the PV response of cells with the I^-/I_3^- couple [73], implying that recombination in working cells does not take place principally at the TCO.

Besides the redox couple and surface properties of the substrate and nanoparticle film, it would be interesting to investigate other factors that influence the locus of recombination in dye-sensitized solar cells. Using IMIS in combination with IMVS and IMPS, a recent study [34] has focused solely on the issue of identifying the locus of recombination in cells containing the I^-/I_3^- couple. From the analysis of the IMIS spectra, the authors conclude that, for the specific cells studied, recombination occurs predominantly near the substrate instead of across the entire TiO_2 film [34]. The cause of this unusual behavior is not understood and requires further study.

4.2. Mechanism

The rate of recombination in dye-sensitized solar cells is approximately second order in the electron density [14,15,31]. The apparent second-order nature of the reaction has been explained by invoking either Scheme 1 (reactions 4.2–4.4) in [15,75] or Scheme 2 (reactions 4.2, 4.3 and 4.5) in [14,31]:

$$I_3^- \overset{K_1}{\longleftrightarrow} I_2 + I^- \tag{4.2}$$

$$I_2 + e \overset{K_2}{\longleftrightarrow} I_2^{\bullet -} \tag{4.3}$$

$$2I_2^{\bullet -} \overset{k_3}{\longrightarrow} I^- + I_3^- \tag{4.4}$$

$$I_2^{\bullet -} + e \overset{k_4}{\longrightarrow} 2I^- \tag{4.5}$$

In both schemes, I_3^- exists in chemical equilibrium with iodide ions in solution and molecular iodine associated with the TiO_2 surface (reaction 4.2). Injected electrons from TiO_2 are presumed to reduce I_2 to the $I_2^{\bullet -}$ radical anion (reaction 4.3) in a second equilibrium [15,75]. The $I_2^{\bullet -}$ radical anion reacts further via dismutation (reaction 4.4 in Scheme 1) or a simple reduction (reaction 4.5 in Scheme 2) as the rate-limiting step. The $I_2^{\bullet -}$ radical anions are also formed in the dye regeneration reaction [76]. If reaction 4.4 (Scheme 1) is rate limiting, the recombination rate R is given by the equation [14,29,31]:

$$R = K_1^2 K_2^2 k_3 \frac{[I_3^-]^2 n^2}{[I^-]^2} \tag{4.6}$$

On the other hand, if reaction 4.5 (Scheme 2) is rate limiting, the recombination rate is [14,29,31]:

$$R = K_1 K_2 k_4 \frac{[I_3^-] n^2}{[I^-]} \tag{4.7}$$

For convenience, we shall refer to both schemes as the *conventional models*. Both models assume that any state in the trap-state distribution can serve as a potential recombination site. In both models, recombination and transport are tacitly assumed to be independent. As both schemes lead to the recombination rate being second order in electron concentration, there has been no definitive experimental evidence based on the reaction order in the electron density that favors one scheme over the other. Also, there has been no conclusive evidence confirming that the reaction rate is second order (Scheme 1) [75] or first order (Scheme 2) [14] in triiodide concentration.

A recent study suggests an alternative explanation for the second order nature of the recombination reaction in the electron density. It is found that both the transport and recombination kinetics are markedly slowed following the intercalation of small amounts of lithium into TiO_2 [29]. Furthermore, transient photocurrent and photovoltage measurements show that the recombination lifetimes of electrons increase in unison with the electron collection (transport) times with increased Li doping of TiO_2 films (Fig. 4) [29], indicating that recombination in *working* dye-sensitized solar cells is limited by electron diffusion in TiO_2, which is contrary to the assumption that dismutation (Eq. (4.4)) or interfacial electron transfer (Eq. (4.5)) is rate limiting. It is not surprising that transport limits recombination when one considers an estimate that there is at most one molecular iodine for every 10^4 TiO_2 nanoparticles in the conventional Grätzel cell [29]. The same temporal correlation between transport and recombination has been observed in dye-sensitized systems without a redox couple, where electrons can recombine only with the oxidized dye [52].

To account for recombination being transport limited in the TiO_2 nanoparticle films, it is assumed that the rate-limiting step (Eq. (4.8)) involves the electron capture by a surface-adsorbed molecular iodine species produced in the chemical equilibrium of I_3^- (Eq. (4.2)) [29]:

$$I_2 + e^- \overset{k_5}{\rightarrow} I_2^{\bullet -} \tag{4.8}$$

which is followed by either the dismutation reaction (Eq. (4.4)) or a second electron capture (Eq. (4.5)). The rate constant of the first electron capture reaction (Eq. (4.8)) is assumed to be proportional to the diffusion coefficient of electrons ($k_5 = C' D_n$, where C' is a constant). The diffusion-limited recombination rate is then written, with the aid of Eq. (3.4) as [29]

$$R \propto D_n n \propto n^{1/\alpha} \tag{4.9}$$

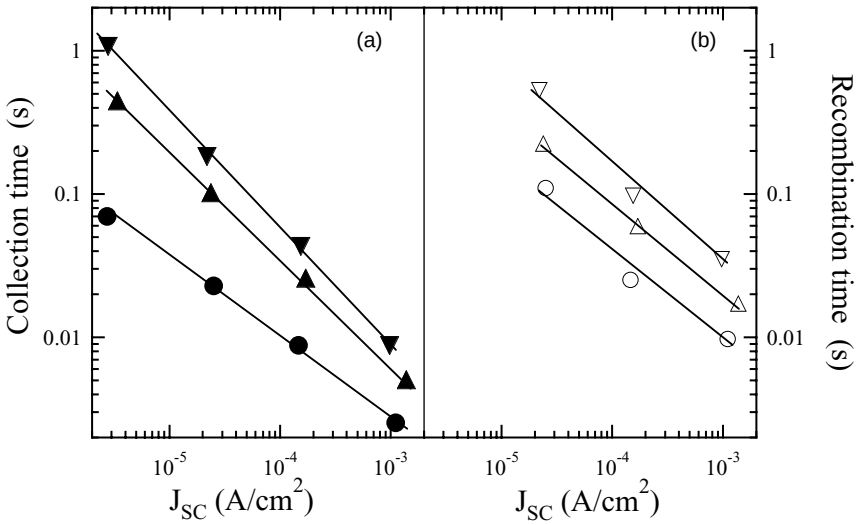

Fig. 4. Dependence of: (a) diffusion and (b) recombination times on short-circuit photocurrent for cells containing an undoped TiO_2 nanoparticle film (circles) and Li-doped TiO_2 nanoparticle films (triangles). The lines are power-law fits to the data. Adapted from [29].

As D_n depends on n (Eq. (3.4)), the recombination rate depends non-linearly on n [29]. Inasmuch as the parameter α, which varies inversely with the average trap depth m_c, is typically about 0.3–0.5 [4,22,23] in the absence of intercalated Li [29], Eq. (4.9) predicts a power-law dependence of the rate of recombination R on the electron density with an exponent value $1/\alpha$ of 2–3, which falls within the range observed for the reaction order [15]. Eq. (4.9) also explains the observed correlation between the recombination rate and the transport rate [29]. In particular, it can be shown by combining the characteristic time for photocarrier recombination τ_r ($\tau_r = n/R$ [31]) and Eq. (4.9) that the recombination time is proportional to the diffusion time (Fig. 4) [29]:

$$\tau_r \propto \tau_c \tag{4.10}$$

It is instructive to examine the physical origin for the dependence of the recombination rate on the electron density from the perspective of the transport-limited model and the conventional models. From the perspective of the transport-limited model, increasing the photocarrier density (light intensity) would result in faster diffusion owing to the progressive filling of deep traps. With faster diffusion, there is a greater probability per unit time that electrons will encounter relatively "rare" and stationary I_2 recombination sites, which, in turn, would lead to faster recombination (Eq. (4.10)). In contrast, in the conventional models, the density of recombination centers does not limit recombination. Instead, the cross-section for a chemical reaction (Eq. (4.4) or (4.5)) limits the rate. Thus, increasing the photocarrier density would increase the probability for the occurrence of a reactive encounter because of the availability of more electrons.

It has been shown that non-intercalated and Li intercalated cells exhibit almost the same open-circuit photovoltages and comparable short-circuit photocurrent densities at one-sun light intensities, despite the marked slowing of both diffusion and recombination in Li doped TiO_2 films [29]. This observation can be understood within the framework of the transport-limited model. As the electron collection and recombination times change in the same manner (Eq. (4.10)), the charge-collection efficiency [9,11] and consequently the short-circuit photocurrent density are predicted to remain relatively unchanged [29]. Furthermore, because the decrease of electron diffusion coefficient in lithium doped films is relatively small at light intensities close to 1 sun (Fig. 4), only a minor increase of V_{oc} ($V_{oc} \propto \ln D_n$) is expected. These results suggest that the solar cell performance will not be significantly improved by enhancing the electron transport rate (i.e., the diffusion coefficient).

As the diffusion limited recombination model accounts for experimental observations better than the conventional models, we currently prefer it to the latter. There is still an unresolved issue common to both the diffusion-limited and conventional recombination models. In the case of the diffusion-limited model, Eq. (4.10) predicts that the electron diffusion length is always constant because the ratio of the recombination lifetime to the transport lifetime is constant. However, it has been reported that the power law dependency of the recombination lifetime differs slightly from that of the transport time [9,14]. This causes a very weak dependence of the diffusion length on light intensity, which results in a factor of two decrease of diffusion length when the light intensity increases by over 4 orders of magnitude [14]. It is likely that this issue can be resolved by a small modification to the diffusion-limited recombination model. For example, one modification could involve consecutive intermediates whereby adsorbed molecular iodine decomposes into iodine atoms associated with the TiO_2 surface. The net effect would be two recombination sites in close proximity.

4.3. Open-circuit photovoltage

The open-circuit photovoltage of the Grätzel cell is defined as the difference between the quasi-Fermi level of electrons in TiO_2 in the light ($\bar{\mu}_n$) and the Fermi level in the dark ($\bar{\mu}_n^0$) [75,77]:

$$V_{oc} = \bar{\mu}_n - \bar{\mu}_n^0 \tag{4.11}$$

Because of equilibration of the TiO_2 film with the TCO substrate and the electrolyte phase, the Fermi level in the dark is the same as the Fermi level of the redox electrolyte, which is constant under illumination at open circuit. As discussed above, the photovoltage of the cell is mainly due to a light-induced change of the chemical potential of electrons in the TiO_2 phase [11,21,78] and, to a lesser extent, a light-induced change of the electrical potential of the TiO_2 particles resulting in band-edge movement [15].

In the absence of band-edge movement (see below), the photoinjected electron density in the conduction band of TiO_2 depends on the dark electron concentration $n_{cb,0}$ and the difference (Eq. (4.11)) between the quasi-Fermi level in the light and the Fermi level in the dark [75]:

$$n_{cb} = n_{cb,0} \exp[q(\bar{\mu}_n - \bar{\mu}_n^0)/kT] \tag{4.12}$$

A similar expression can be written for the total photoinjected electron density n when electrons reside predominantly in an exponential distribution of traps (Eq. (3.10)):

$$n = n_{t,0} \exp[q(\bar{\mu}_n - \bar{\mu}_n^0)/m_c] \tag{4.13}$$

where m_c is the characteristic energy of the exponential trap-state distribution [15] and $n_{t,0}$ the trapped electron density in the dark. The latter expression shows that the average trap depth can be determined from measurements of the electron charge in the film versus the open-circuit voltage [15]. Measurements of m_c from the voltage dependence of the photoinjected charge [9] and from the transport kinetics [4,12,22,23] are in reasonable agreement. The values for m_c determined from the voltage measurements are, however, systematically slightly higher than those obtained from transport measurements [4,12,22,23], which is probably due to the same phenomenon causing the electron diffusion length to depend on the light-intensity (Section 4.2).

4.4. Band-edge movement

Normally, at a constant photoinjected charge density, the open-circuit photovoltage is fixed (Eq. (4.11)) even if, for example, the electron transfer rate constant were altered by chemically shielding (passivating) the TiO_2 surface against recombination [15,75]. An exception to this behavior occurs in the case of band-edge movement. Fig. 5 illustrates this concept for a conduction band-edge shift to negative potentials, which would increase the photovoltage even at a constant photocharge density [15]. This shift in band edge can be induced by chemically treating the surface [15] or by exposing the cell to sufficiently high light intensities [15,35].

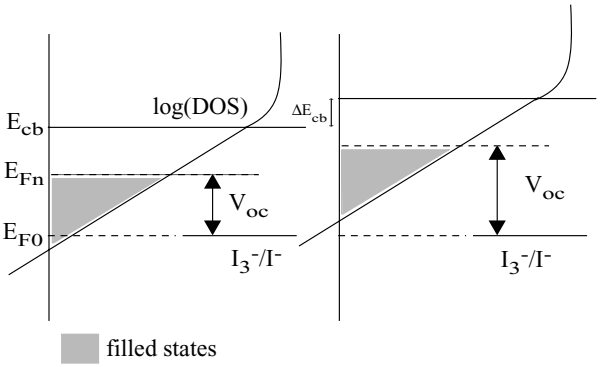

Fig. 5. Effect of conduction band-edge position E_{cb} on the open-circuit voltage V_{oc} for a fixed exponential trap density at the same photoinduced charge density. Band-edge shift from (a) to (b) increases the open-circuit photovoltage of cell with no effect on trap filling (grey region) by photoinjected electrons.

The effects of band-edge movement on the open-circuit photovoltage and the recombination kinetics in the Grätzel cell were first demonstrated several years ago when it was shown that treating the TiO_2 surface with 4-*tert*-butylpyridine or ammonia causes a significant negative potential shift of the band edges resulting in an increased open-circuit voltage at constant photoinduced charge (Fig. 6). The band-edge shift was attributed to the amines charging the TiO_2 surface negatively by deprotonating it [15]. Lower photovoltages have resulted from adding adsorptive cations, such as Li^+, to the electrolyte, which are presumed to charge the surface positively resulting in the band-edge shift to positive potentials [79]. Band-edge movement also affects the recombination lifetime of electrons. For example, it has been shown that if the band edges shift to negative potentials, the recom-

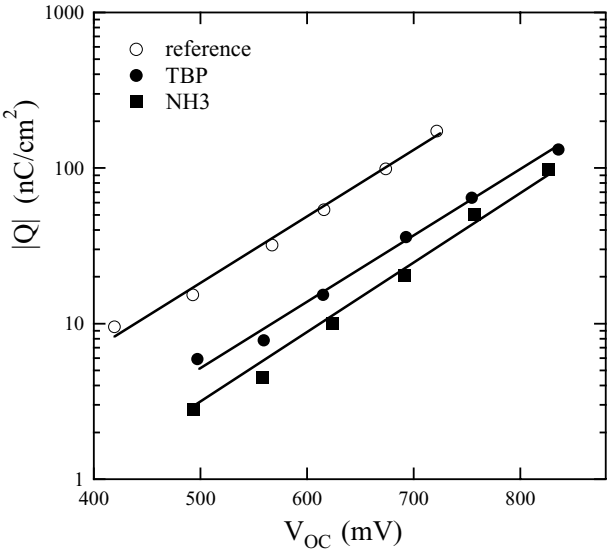

Fig. 6. Dependence of photoinjected charge density $|Q|$ on open-circuit photovoltage for untreated (reference) and TBP (4-*tert*-butylpyridine) and NH_3 treated dye-sensitized TiO_2 nanoparticle films. Lines are fits to data. Adapted from [15].

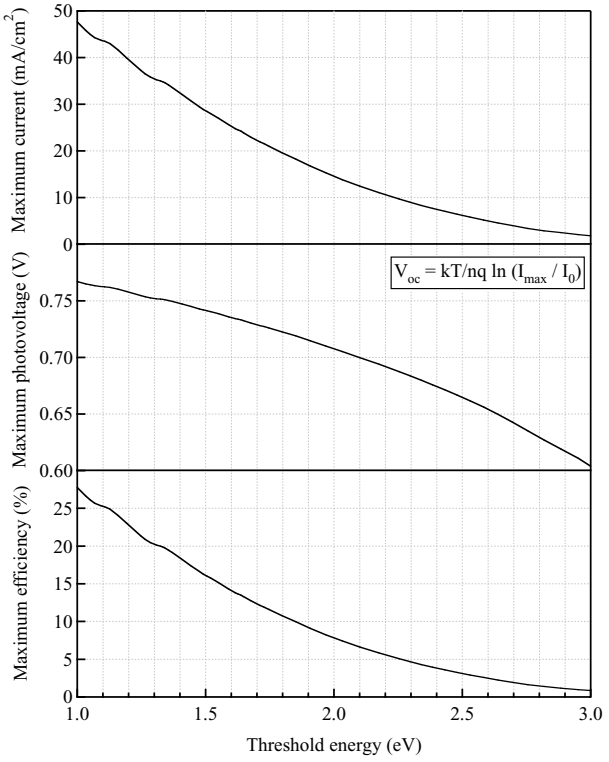

Fig. 7. Theoretical short-circuit photocurrent, open-circuit photovoltage, and efficiency vs. excitation energy of an ideal Grätzel cell with the standard triiodide/iodide redox couple. No surface recombination loss and reflection loss of incident light are assumed. Diode ideality factor of 1.9 is assumed.

bination of electrons at a *fixed* V_{oc} becomes slower owing to a decrease of the trapped electron density in the dark $n_{t,0}$ [15]. Besides negative potential shifts of the conduction band edge, passivating the TiO_2 surface is also expected to increase V_{oc} by lowering the cross section for electron capture by adsorbed molecular iodine and, therefore, increasing the photoinjected charge.

5. PV properties

In this section, we examine the fundamental factors that limit the PV performance of dye-sensitized solar cells. The overall solar conversion efficiency η is determined from the short-circuit photocurrent, the open-circuit photovoltage, and the fill factor FF.

$$\eta = \frac{P_{out}}{P_{in}} = \frac{V_{oc}|J_{sc}|FF}{P_{in}} \quad (5.1)$$

where P_{in} is the total solar input power and P_{out} the power density of the cell at the maximum power point. Typical values for the fill factor range from 0.65 to 0.75. Fig. 7 shows the theoretical short-circuit photocurrent and efficiency of a dye-sensitized solar cell incorporating the standard triiodide/iodide redox couple for a range of photovoltages (0.7–0.8 V) that have been measured. The maximum short-circuit photocurrent J_{sc}^{max} was determined from integrating the terrestrial solar spectrum [80] for air mass (AM) 1.5 (the power flux in the sunlight is 1000 W/m^2 at AM 1.5), corresponding to the situation where every photon with energy equal to or above the excitation threshold of the sensitizer (absorber) contributes to the photocurrent. The open-circuit photovoltage V_{oc} can be obtained from the diode equation:

$$J_{sc} = J_0 \exp[qV_{oc}/\beta kT] \quad (5.2)$$

where β is the diode ideality factor and J_0 the dark exchange current; negligible series resistance losses are assumed. For dye-sensitized solar cells, values of β range from 1.5 to 2 [7,11,75,81], which has been attributed to the resistance associated with electron transfer across the TiO_2–redox electrolyte interface [11]. For convenience, we assume an average β value of 1.9. The value of J_0 can vary, depending on the sensitizers and other components of the cells. For example, from *J–V* data for dye-sensitized solar cells with state-of-the art sensitizers [82–84], such as N719 dye (*cis*-Ru[LL′(NCS)$_2$] (L=2,2′-bypyridyl-4,4′-dicarboxylic acid, L′ = 2,2′-bipyridyl-4,4′-ditetrabutylammoniumcarboxylate)) and the black dye (tri(cyanato)-2,2′,2″-terpyridyl-4,4′,4″-tricarboxylate)Ru(II)), we determined J_0 values of 7.8–11.0 nA/cm^2. The maximum efficiency η^{max} is calculated from J_{sc}^{max} and V_{oc} values (Fig. 7) and a fill factor of 0.76, which is within the range of values observed in efficient dye-sensitized solar cells. The relatively low value of the fill factor is due to a diode ideality factor of 1.9.

It is informative to compare the theoretical efficiencies with those of the most efficient dye-sensitized solar cells and then to examine the factors that limit their efficiency. The two highest overall confirmed efficiencies of a dye-sensitized solar cell has been achieved with two different sensitizers, the N719 dye and the black dye [82,83]. Under full sunlight (AM 1.5), the confirmed efficiency of the N719-sensitized cell was 10% [82] and that of the black dye-sensitized cell was 10.4% [83]. From Fig. 7, a cell with the same photocurrent threshold as the black dye (920 nm (1.348 eV) [85]) would display a much higher short-circuit photocurrent and efficiency than those of the record setting black dye-sensitized solar cell. The short-circuit photocurrent would increase from 20.53 to 34.4 mA/cm^2, the open-circuit photovoltage would increase from 0.721 to 0.750 V, and the fill factor would increase from 0.7041 to 0.760. With these values of the J_{sc}, V_{oc}, and FF in Fig. 7, the overall cell efficiency would increase from 10.4 to 19.6%. The corresponding overall efficiency of the N719-sensitized cell, which has a photocurrent onset at 1.59 eV (780 nm) [84], is 14.3%.

There has been no dye-sensitized solar cell that has achieved a confirmed short-circuit photocurrent at AM 1.5 solar radiation above 25 mA/cm^2, which is substantially below the theoretical maximum photocurrent. Besides the incident solar flux, the principal fundamental factor that limits the short-circuit photocurrent is the incident photon-to-current conversion efficiency (IPCE), which is

determined by the product of the light-harvesting efficiency of the dye (η_{lh}), the quantum yield of electron injection (η_{inj}), and the efficiency of collecting the injected electrons (η_{cc}) at the transparent back contact [9]. These three efficiencies (η_{lh}, η_{inj}, η_{cc}) convert the incident solar flux to the steady-state electron density at short circuit. A low IPCE is the result of either inefficient light harvesting by the dye, inefficient charge injection into TiO_2, or inefficient collection of injected electrons. Specific causes for low η_{lh}, η_{inj} and η_{cc} have been discussed, in part, elsewhere [81]. A low η_{lh} can be due to, for example, a low dye absorption coefficient over the solar spectrum, a low dye concentration, a TiO_2 film too thin to support an adsorbed dye concentration that absorbs a significant fraction of the incident light, insufficient light scattering within the film, absorption of light by TiO_2 or the redox electrolyte, and dye degradation. A low η_{inj} can be due to, for instance, dye desorption, dye aggregation or the excited state levels of the dye lying below the conduction band edge of TiO_2. A low η_{cc} is due to competition between fast recombination of photoinjected electrons with the redox electrolyte or oxidized dye and electron collection. It is difficult experimentally to determine which of the three efficiencies (light absorption, charge injection, and charge collection) limit the IPCE. We have developed, however, a simple analytical expression to determine the charge-collection efficiency as a function of applied bias from the time constants for recombination and charge collection ($\tau_r/\tau_c = (1 - \eta_{cc})^{-1}$) [11].

In general, even in the most efficient cells, the IPCE is less than unity at short circuit even for monochromatic light. This stems from the fact that the light-harvesting efficiency is not unity even at the maximum of the spectral response of the dye, let alone over the solar spectrum, for reasons discussed above, for instance, the attenuation of light by the redox electrolyte. Also, with few exceptions, the charge-injection efficiency is less than unity over the solar spectrum because the distribution of donor electronic levels of the excited state of the dye does not, in general, lie entirely above the conduction band edge (Fig. 8). Furthermore, one would anticipate that in the few cases where the distribution of electronic levels of the excited state of the dye lies above the conduction band edge, either the photocurrent or photovoltage would be substantially below the theoretical maximum. For the conduction band edge to lie below the excited state of the dye, either the excitation threshold of the dye must be of sufficiently high energy that the light-harvesting efficiency of the dye would suffer or the position of the conduction band edge energy must be shifted to lower energy. The use of a lithium electrolyte would induce the latter situation [79,86]. In contrast to the light-harvesting efficiency and the charge-injection efficiency, a charge-collection efficiency close to unity is achievable experimentally by reducing the rate of recombination. The fact that the experimentally observed open-circuit photovoltage is close to the theoretical maximum V_{oc} for a given solar flux indicates that electron collection competes favorably with recombination in the most efficient cells. It is important to emphasize, however, that the charge-collection efficiency for less efficient cells, solid-state cells or other arrangements involving non-standard redox couples, photosensitizers, etc. may be substantially less than unity.

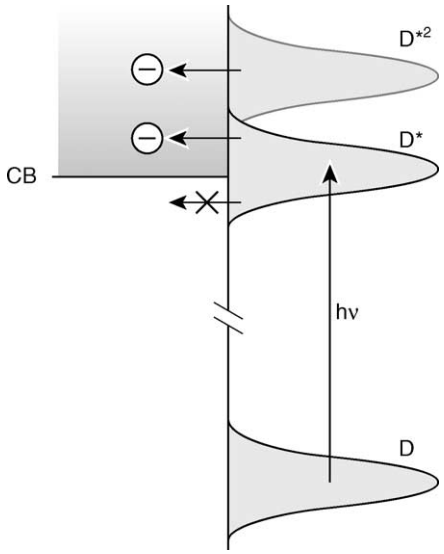

Fig. 8. Schematic representation of distribution of donor electronic energy levels of adsorbed dye on TiO_2 involved in electron injection.

The open-circuit photovoltage is determined by the difference between the quasi-Fermi level (electrochemical potential) in the light and the Fermi level in the dark (Eq. (4.11)). The quasi-Fermi level in the light (electron quasi-Fermi level at the back contact) is controlled by the light-harvesting efficiency of the dye, the quantum yield of electron injection and the time constant for recombination with the electron acceptor (redox species, oxidized dye). These two efficiencies (η_{lh}, η_{inj}) and the recombination time constant convert the incident light intensity into the steady-state electron density at open circuit.

The fill factor is a phenomenological quantity, which depends on the series resistance of the cell, which is the sum of the sheet resistances of the conducting glass substrate and counter electrode, the resistance of the substrate–TiO_2 interface, the resistance associated with ion transport in the electrolyte, the charge-transfer resistance at the counter electrode, and the voltage dependence of the recombination rate. The charge-transfer resistance at the counter electrode is affected by the redox activity of the Pt (or graphite) catalyst toward oxidized redox species, the electrolyte, the solvent, and concentration of the oxidized redox species (e.g., I_3^-) [87].

6. Summary

In high ionic strength electrolytes, the electrical field generated by electrons in the TiO_2 layer is screened at normal solar light intensities, except for a small region within

one nanoparticle layer adjacent to the TCO substrate. The enormous discrepancy between the ion density (typically on the order of $10^{20}\,cm^{-3}$) in the electrolyte and the electron density (at or below $10^{18}\,cm^{-3}$ at one-sun light intensity) in the TiO_2 layer has several important consequences on electron transport in the conventional Grätzel cell: (1) electron motion is essentially diffusional; (2) diffusion is ambipolar; and (3) the measured current arising from charge transport is detected only when electrons arrive at the collecting electrode. The nanoparticle film morphology strongly influences electron transport. Changing the film porosity from 50 to 75% causes, for instance, the electron path length to increase 10-fold, which, in a 10 μm thick film, amounts to an increase from 10^6 to 10^7 particles. The defect structure of the TiO_2 film also has a major influence on electron transport. Evidence connecting the non-linear light-intensity dependence of the electron transport and recombination kinetics in the film with multiple trapping in an exponential distribution of traps is discussed. At light intensities of about one-sun, an electrical field is created across the TiO_2 layer leading to a significant enhancement (2–20%) of the apparent diffusion coefficient. The additional driving force is expected to become important for high efficiency cells or cells operating above one-sun light intensity (electron density $> 10^{18}\,cm^{-3}$). The relatively slow recombination kinetics of the I_3^-/I^- redox couple is a major reason for the good performance of the Grätzel cell. Efforts to understand the principal factors that determine the recombination kinetics and their relation to the cell performance have involved a combination of theoretical and experimental approaches. The interface, where recombination predominates, depends on the spatial region of photoinjected charge buildup in the cell, the redox electrolyte, and the surface properties of both the TiO_2 nanoparticle film and the TCO substrate. The photocharge builds up in the TiO_2 film, and, in the case of the I_3^-/I^- redox couple, recombination occurs predominately at the TiO_2–electrolyte interface. The consensus of several studies is that the buildup of charge also creates the photovoltage of the Grätzel cell by raising the Fermi level in the TiO_2 film. Three recombination mechanisms have been proposed to account for the exponential dependence of the rate of recombination on the photocharge density. A critical difference among them is the assignment of the rate-limiting step. Two of the mechanisms assume either a dismutation reaction or an interfacial electron transfer reaction as rate-limiting. The third mechanism is based on a more recent study, which indicates that electron transport limits recombination. This latter view has significant implications on the physical origin for recombination and on the choice of approaches to improve cell performance. It is assumed that recombination is causally linked to electrons encountering relatively "rare" surface sites involving an iodine intermediate. From this perspective, the factors that limit the transport dynamics also influence the recombination kinetics. The results of this study also imply that making electrons move faster will not significantly improve the cell performance.

Acknowledgements

This work was supported by the Office of Science, Division of Chemical Sciences, and the Office of Utility Technologies, Division of Photovoltaics, US Department of Energy, under contract DE-AC36-99GO10337.

References

[1] B. O'Regan, M. Grätzel, Nature 353 (1991) 737.
[2] M. Grätzel, A.J. Frank, J. Phys. Chem. 86 (1982) 2964.
[3] A. Hagfeldt, M. Grätzel, Chem. Rev. 95 (1995) 49.
[4] K.D. Benkstein, N. Kopidakis, J. van de Lagemaat, A.J. Frank, J. Phys. Chem. B 107 (2003) 7759.
[5] F. Cao, G. Oskam, G.J. Meyer, P.C. Searson, J. Phys. Chem. 100 (1996) 17021.
[6] P.E. de Jongh, D. Vanmaekelbergh, Phys. Rev. Lett. 77 (1996) 3427.
[7] L. Dloczik, O. Ileperuma, I. Lauermann, L.M. Peter, E.A. Ponomarev, G. Redmond, N.J. Shaw, I. Uhlendorf, J. Phys. Chem. B 101 (1997) 10281.
[8] P.E. de Jongh, D. Vanmaekelbergh, J. Phys. Chem. B 101 (1997) 2716.
[9] G. Schlichthörl, N.-G. Park, A.J. Frank, J. Phys. Chem. B 103 (1999) 782.
[10] D. Vanmaekelbergh, P.E. de Jongh, Phys. Rev. B 61 (2000) 4699.
[11] J. van de Lagemaat, N.-G. Park, A.J. Frank, J. Phys. Chem. B 104 (2000) 2044.
[12] J. van de Lagemaat, A.J. Frank, J. Phys. Chem. B 104 (2000) 4292.
[13] A. Kambili, A.B. Walker, F.L. Qiu, A.C. Fisher, A.D. Savin, L.M. Peter, Phys. E 14 (2002) 203.
[14] A.C. Fisher, L.M. Peter, E.A. Ponomarev, A.B. Walker, K.G.U. Wijayantha, J. Phys. Chem. B 104 (2000) 949.
[15] G. Schlichthörl, S.Y. Huang, J. Sprague, A.J. Frank, J. Phys. Chem. B 101 (1997) 8141.
[16] T. Dittrich, J. Weidmann, V.Y. Timoshenko, A.A. Petrov, F. Koch, M.G. Lisachenko, E. Lebedev, Mater. Sci. Eng. B 69/70 (2000) 489.
[17] F. Fabregat-Santiago, G. Garcia-Belmonte, J. Bisquert, A. Zaban, P. Salvador, J. Phys. Chem. B 106 (2002) 334.
[18] R. Kern, R. Sastrawan, J. Ferber, R. Stangl, J. Luther, Electrochim. Acta 47 (2002) 4213.
[19] J. Bisquert, G. Garcia-Belmonte, F. Fabregat-Santiago, N.S. Ferriols, P. Bogdanoff, E.C. Pereira, J. Phys. Chem. B 104 (2000) 2287.
[20] K. Schwarzburg, F. Willig, J. Phys. Chem. B 107 (2003) 3552.
[21] G. Kron, T. Egerter, J.H. Werner, U. Rau, J. Phys. Chem. B 107 (2003) 3556.
[22] N. Kopidakis, E.A. Schiff, N.-G. Park, J. van de Lagemaat, A.J. Frank, J. Phys. Chem. B 104 (2000) 3930.
[23] J. van de Lagemaat, A.J. Frank, J. Phys. Chem. B 105 (2001) 11194.
[24] A. Solbrand, H. Lindström, H. Rensmo, A. Hagfeldt, S.-E. Lindquist, J. Phys. Chem. B. 101 (1997) 2514.
[25] K. Schwarzburg, F. Willig, Appl. Phys. Lett. 58 (1991) 2520.
[26] A. Solbrand, A. Henningsson, S. Södergren, H. Lindström, A. Hagfeldt, S.-E. Lindquist, J. Phys. Chem. B 103 (1999) 1078.
[27] T. Dittrich, Phys. Status Solidi A 182 (2000) 447.
[28] T. Dittrich, E.A. Lebedev, J. Weidmann, Phys. Status Solidi A 165 (1998) R5.
[29] N. Kopidakis, K.D. Benkstein, J. van de Lagemaat, A.J. Frank, J. Phys. Chem. B 107 (2003) 11307.
[30] T. Dittrich, V. Duzhko, F. Kock, V. Kytin, J. Rappich, Phys. Rev. B 65 (2002) 155319.
[31] N.W. Duffy, L.M. Peter, R.M.G. Rajapakse, K.G.U. Wijayantha, J. Phys. Chem. B 104 (2000) 8916.
[32] A. Zaban, M. Greenshtein, J. Bisquert, Chem. Phys. Chem. 4 (2003) 859.

[33] G. Franco, J. Gehring, L.M. Peter, E.A. Ponomarev, I. Uhlendorf, J. Phys. Chem. B 103 (1999) 692.
[34] K. Zhu, E.A. Schiff, N.-G. Park, J. van de Lagemaat, A.J. Frank, Appl. Phys. Lett. 80 (2002) 685.
[35] D. Vanmaekelbergh, P.E. de Jongh, J. Phys. Chem. B 103 (1999) 747.
[36] J. Ferber, J. Luther, J. Phys. Chem. B 105 (2001) 4895.
[37] A. Zaban, A. Meier, B. Gregg, J. Phys. Chem. B 101 (1997) 7985.
[38] D. Nistér, K. Keis, S.-E. Lindquist, A. Hagfeldt, Sol. Energy Mater. Sol. Cells 73 (2002) 411.
[39] J.-F. Dufrêche, O. Bernard, O. Turq, J. Chem. Phys. 116 (2002) 2085.
[40] S.M. Sze, Semiconductor Devices. Physics and Technology, John Wiley & Sons, New York, 1985.
[41] W. van Roosbroeck, Phys. Rev. 91 (1953) 282.
[42] S. Kambe, S. Nakade, T. Kitamura, Y. Wada, S. Yanagida, J. Phys. Chem. B 106 (2002) 2967.
[43] S. Nakade, S. Kambe, T. Kitamura, Y. Wada, S. Yanagida, J. Phys. Chem. B 105 (2001) 9150.
[44] J.R. Haynes, W. Shockley, Phys. Rev. 81 (1951) 835.
[45] N.-G. Park, J. van de Lagemaat, A.J. Frank, J. Phys. Chem. B 104 (2000) 8989.
[46] M.J. Cass, F.L. Qiu, A.B. Walker, A.C. Fisher, L.M. Peter, J. Phys. Chem. B 107 (2003) 113.
[47] J. van de Lagemaat, K.D. Benkstein, A.J. Frank, J. Phys. Chem. B 105 (2001) 12433.
[48] L. Forro, O. Chauvet, A. Emin, L. Zuppiroli, H. Berger, F. Levy, J. Appl. Phys. 75 (1994) 633.
[49] H. Scher, M. Lax, Phys. Rev. B 7 (1973) 4491.
[50] H. Scher, E.W. Montroll, Phys. Rev. B 12 (1975) 2455.
[51] J. Nelson, Phys. Rev. B 59 (1999) 15374.
[52] J. Nelson, S.A. Haque, D.R. Klug, J.R. Durrant, Phys. Rev. B 63 (2001) 205321.
[53] N.F. Mott, Philos. Mag. 34 (1976) 643.
[54] T. Tiedje, J.M. Cebulka, D.L. Morel, B. Abeles, Phys. Rev. Lett. 46 (1981) 1425.
[55] F. Meng, C. Rongqiang, W.Z. Shen, J. Appl. Phys. 90 (2001) 3387.
[56] R.L. Willis, C. Olson, B. O'Regan, T. Lutz, J. Nelson, J.R. Durrant, J. Phys. Chem. B 106 (2002) 7605.
[57] A.L. Roest, P.E. de Jongh, D. Vanmaekelbergh, Phys. Rev. B 62 (2000) 16926.
[58] K. Takeshita, Y. Sasaki, M. Kobashi, Y. Tanaka, S. Maeda, J. Phys. Chem. B 107 (2003) 4156.
[59] K. Westermark, A. Henningsson, H. Rensmo, S. Sodergren, H. Siegbahn, A. Hagfeldt, Chem. Phys. 285 (2002) 157.
[60] N.M. Dimitrijevic, Z.V. Saponjic, D.M. Bartels, M.C. Thurnauer, D.M. Tiede, T. Rajh, J. Phys. Chem. B 107 (2003) 7368.
[61] S.H. Szczepankiewicz, J.A. Moss, M.R. Hoffmann, J. Phys. Chem. B 106 (2002) 2922.
[62] W. Göpel, G. Rocker, R. Feierabend, Phys. Rev. B 28 (1983) 3427.
[63] J.I. Pankove, Optical Processes in Semiconductors, Dover Publications, New York, 1971.
[64] M. Silver, L. Pautmeier, H. Bässler, Sol. State Commun. 72 (1989) 177.
[65] H. Tang, F. Levy, H. Berger, P.E. Schmid, Phys. Rev. B 52 (1995) 7771.
[66] J.A. Anta, J. Nelson, N. Quirke, Phys. Rev. B 65 (2002).
[67] L. Onsager, R.M. Fuoss, J. Phys. Chem. 36 (1932) 2689.
[68] B.A. Gregg, J. Phys. Chem. B 107 (2003) 4688.
[69] A. van der Ven, G. Ceder, M. Asta, P.D. Tepesch, Phys. Rev. B 64 (2001).
[70] J. Bisquert, J. Phys. Chem. B 108 (2004) 2323.
[71] S.A. Haque, Y. Tachibana, D.R. Klug, J.R. Durrant, J. Phys. Chem. B 102 (1998) 1745.
[72] S.A. Haque, Y. Tachibana, R.L. Willis, J.E. Moser, M. Grätzel, D.R. Klug, J.R. Durrant, J. Phys. Chem. B 104 (2000) 538.
[73] B.A. Gregg, F. Pichot, S. Ferrere, C.L. Fields, J. Phys. Chem. B 105 (2001) 1422.
[74] F. Cao, G. Oskam, P.C. Searson, J.M. Stipkala, T.A. Heimer, F. Farzad, G.J. Meyer, J. Phys. Chem. 99 (1995) 11974.
[75] S.Y. Huang, G. Schlichthörl, A.J. Nozik, M. Grätzel, A.J. Frank, J. Phys. Chem. B 101 (1997) 2576.
[76] I. Montanari, J. Nelson, J.R. Durrant, J. Phys. Chem. B 106 (2002) 12203.
[77] E.A. Schiff, Sol. Energy Mater. Sol. Cells 78 (2003) 567.
[78] F. Pichot, B.A. Gregg, J. Phys. Chem. B 104 (2000) 6.
[79] N.-G. Park, S.-H. Chang, J. van de Lagemaat, K.-J. Kim, A.J. Frank, Bull. Korean Chem. Soc. 21 (2000) 985.
[80] ASTM G159-98, Standard Tables for References Solar Spectral Irradiance at Air Mass 1.5: Direct Normal and Hemispherical for a 37° Tilted Surface, Annual Book of ASTM Standards 1998, vol. 14.04, American Society for Testing and Materials, West Conshohocken, PA.
[81] S. Södergren, A. Hagfeldt, J. Olsson, S.-E. Lindquist, J. Phys. Chem. 95 (1994) 5522.
[82] C.J. Barbé, F. Arendse, P. Comte, M. Jirousek, F. Lenzmann, V. Shklover, M. Grätzel, J. Am. Ceram. Soc. 80 (1997) 3157.
[83] M.K. Nazeeruddin, P. Pechy, T. Renouard, S.M. Zakeeruddin, R. Humphry-Baker, P. Comte, P. Liska, L. Cevey, E. Costa, V. Shklover, L. Spiccia, G.B. Deacon, C.A. Bignozzi, M. Grätzel, J. Am. Chem. Soc. 123 (2001) 1613.
[84] M.K. Nazeeruddin, R. Splivallo, P. Liska, P. Comte, M. Grätzel, Chem. Commun. 12 (2003) 1456.
[85] M.K. Nazeeruddin, P. Pechy, M. Grätzel, Chem. Commun. 18 (1997) 1075.
[86] Y. Liu, A. Hagfeldt, X.-R. Xiao, S.-E. Lindquist, Sol. Energy Mater. Sol. Cells 55 (1998) 267.
[87] A. Hauch, A. Georg, Electrochim. Acta 46 (2001) 3457.